PRECLINICAL RESEARCH

Electroanatomical Navigation to Minimize Contrast Medium or X-Rays During Stenting

Insights From an Experimental Model

Jean-François Dorval, MD,[a,b] Louis-Philippe Richer, PhD,[c] Luc Soucie, PhD,[d] Luke C. McSpadden, PhD,[c]
Adam Hoopai, BSc,[e] Stéphanie Tan, MD,[f] Nick E.J. West, MD,[e] E. Marc Jolicoeur, MD, MSc, MHS[b,g]

VISUAL ABSTRACT

Dorval, J.-F. et al. J Am Coll Cardiol Basic Trans Science. 2022;7(2):131–142.

HIGHLIGHTS

- Contrast media and x-rays used in vascular interventional procedures have been linked to health hazards for patients and medical teams.

- Modified OCT and angioplasty catheters were successful navigated in coronary and carotid arteries using an impedance-sensitive navigation system and used to precisely deliver and implant stents in specified arterial targets without the need for x-ray or contrast medium. Our system achieved an accuracy of 90% and a precision of 1.4mm.

- This proof-of-principle experiment opens the door to PCI with no contrast medium or X-ray in human through the integration of coronary CT scan and intracoronary imaging technologies within navigation systems.

From the [a]Interventional Cardiology Service, Montreal Heart Institute, Montréal, Québec, Canada; [b]Université de Montréal, Montréal, Québec, Canada; [c]Abbott CAHF, Sylmar, California, USA; [d]Abbott, Mississauga, Ontario, Canada; [e]Abbott Vascular, Santa Clara, California, USA; [f]Department of Radiology, Montreal Heart Institute, Montréal, Québec, Canada; and the [g]Service d'Hémodynamie, Centre Hospitalier de l'Université de Montréal, Montréal, Québec, Canada.

ABBREVIATIONS AND ACRONYMS

3D = 3-dimensional

3DGeo$_{CT}$ = 3-dimensional geometry derived from computed tomographic imaging

CMR = cardiovascular magnetic resonance

CTA = computed tomographic angiography

IQR = interquartile range

OCT = optical coherence tomography

ABSTRACT

Stents can be effectively implemented with no x-rays or contrast medium. Modified stents were successfully implanted in 9 of 11 attempted targets (82%) (7 carotid and 4 coronary arteries) using an impedance-sensitive navigation system and optical coherence tomography. Electroanatomical navigation systems can be used to assist interventionalists in performing arterial stenting while minimizing x-ray and contrast use, thereby potentially enhancing safety for both patients and catheterization laboratory staff members.

(J Am Coll Cardiol Basic Trans Science 2022;7:131–142) © 2022 The Authors. Published by Elsevier on behalf of the American College of Cardiology Foundation. This is an open access article under the CC BY-NC-ND license (http://creativecommons.org/licenses/by-nc-nd/4.0/).

Stenting relies on imaging using iodine-based contrast media and x-rays, both of which are linked to health hazards for patients and medical teams. Iodine-based contrast is nephrotoxic and can trigger acute renal failure or the need for dialysis. Furthermore, radiation dose from x-rays required during a percutaneous intervention are lifetime cumulative with other medical ionizing radiation and have been linked with neoplasia in patients [1]. Exposure to x-rays and proximity to imaging equipment have also been linked to left-sided brain tumors or eye lens opacities among catheterization laboratory staff members [2,3].

Modern mitigation strategies exist to minimize radiation dose and contrast use in uncomplicated stenting procedures, included zero-contrast percutaneous coronary intervention [4], coregistration, staged interventions [5] or robotic-assisted percutaneous coronary intervention [6], and a variety of adjunctive shielding tools. A technological innovation capable of mitigating the requirement for contrast and x-ray use during vascular imaging and interventions bears the potential to improve the safety of patients and health care teams alike and to disrupt the field of vascular intervention significantly.

In the past decade, navigation systems have emerged as an adjunct to fluoroscopy for complex procedures in cardiac electrophysiology [7] and structural heart intervention [8]. These systems incorporate distinct imaging modalities into computerized electroanatomical mapping, which allows safe real-time navigation of diagnostic tools or therapeutic devices inside the heart without the need for fluoroscopic guidance. These systems have drastically reduced radiation exposure without compromising procedural accuracy or adding to procedural duration in numerous electrophysiology programs [9]. Interventional cardiologists and radiologists rely heavily on fluoroscopy, with no viable alternatives. Although navigation systems have shown utility and safety in larger cardiac chambers, limited evidence suggests that these systems could work properly in arteries [10]. Weisz et al [11], for instance, were able to project and precisely track a magnetic medical positioning system on recorded cine loops and 3-dimensional (3D) reconstructions acquired from real-time fluoroscopy in patients.
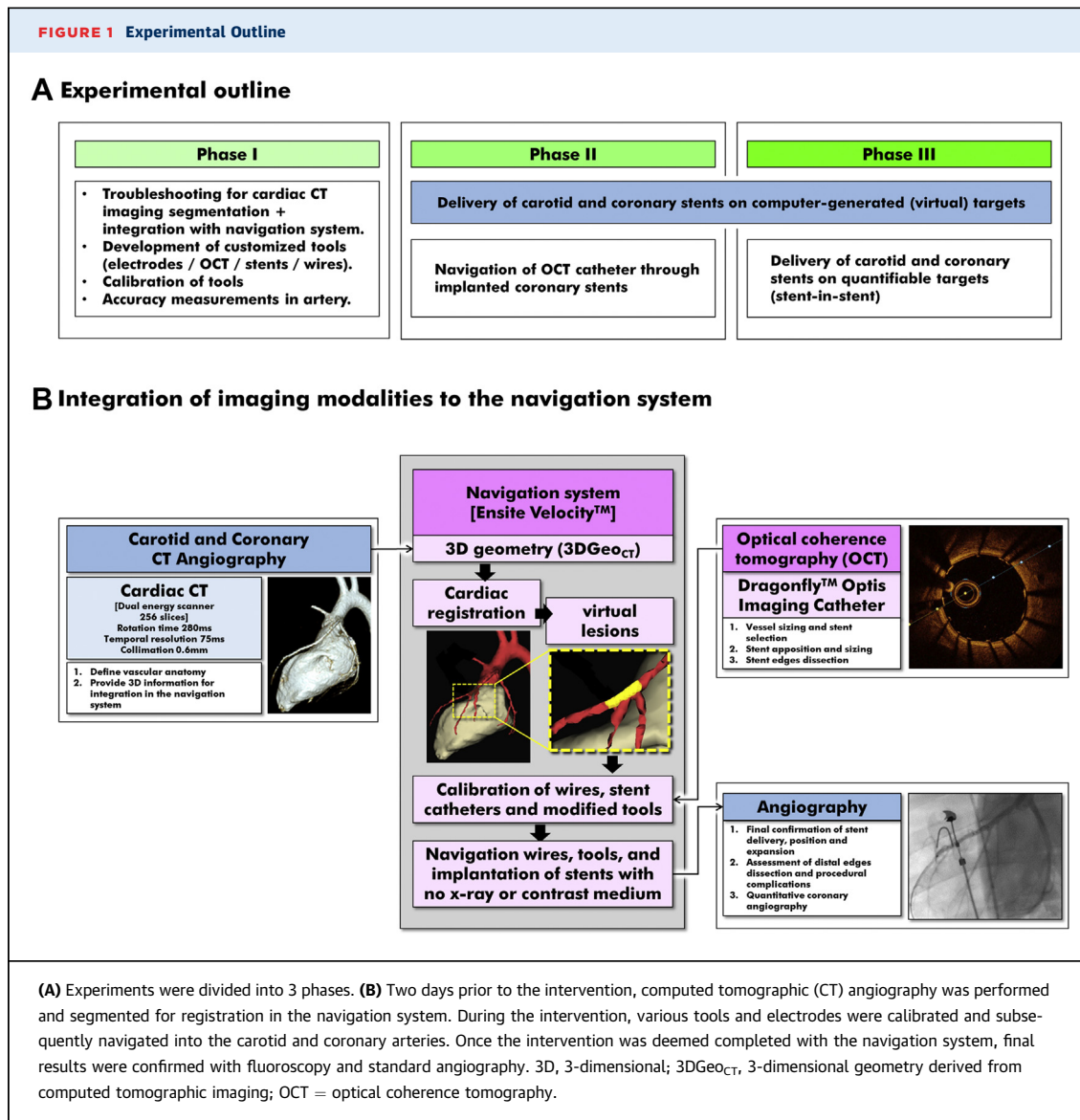
We hypothesized that navigation systems can be used in the future to navigate enabled devices and deliver stents without any contrast agent or x-rays. The capability of an impedance cardiac navigation system to provide accurate tracking and positioning information to guide interventional tools for millimetric interventions remains to be tested. To this end, we tested the feasibility of using an electroanatomical navigation system to deliver stents to minimize the use of both contrast agent and x-rays in the coronary and carotid arteries in a porcine model.

METHODS

STUDY OUTLINE AND POPULATION. The aim of this proof-of-concept study was to assess the feasibility of delivering stents using an electroanatomical navigation system on arterial targets (**Figure 1**). To this end, the experiments were divided into 3 phases, which were reflective of: 1) the degree of integration of customized tools with the navigation system; and 2) the progress of our procedural skills using this novel technique. The aim of the first phase was to

FIGURE 1 Experimental Outline

A Experimental outline

Phase I	Phase II	Phase III
• Troubleshooting for cardiac CT imaging segmentation + integration with navigation system. • Development of customized tools (electrodes / OCT / stents / wires). • Calibration of tools • Accuracy measurements in artery.	Delivery of carotid and coronary stents on computer-generated (virtual) targets	
	Navigation of OCT catheter through implanted coronary stents	Delivery of carotid and coronary stents on quantifiable targets (stent-in-stent)

B Integration of imaging modalities to the navigation system

Carotid and Coronary CT Angiography

Cardiac CT
[Dual energy scanner
256 slices]
Rotation time 280ms
Temporal resolution 75ms
Collimation 0.6mm
1. Define vascular anatomy
2. Provide 3D information for integration in the navigation system

Navigation system [Ensite Velocity™]
3D geometry (3DGeo_CT)
Cardiac registration → virtual lesions
Calibration of wires, stent catheters and modified tools
Navigation wires, tools, and implantation of stents with no x-ray or contrast medium

Optical coherence tomography (OCT)
Dragonfly™ Optis Imaging Catheter
1. Vessel sizing and stent selection
2. Stent apposition and sizing
3. Stent edges dissection

Angiography
1. Final confirmation of stent delivery, position and expansion
2. Assessment of distal edges dissection and procedural complications
3. Quantitative coronary angiography

(A) Experiments were divided into 3 phases. (B) Two days prior to the intervention, computed tomographic (CT) angiography was performed and segmented for registration in the navigation system. During the intervention, various tools and electrodes were calibrated and subsequently navigated into the carotid and coronary arteries. Once the intervention was deemed completed with the navigation system, final results were confirmed with fluoroscopy and standard angiography. 3D, 3-dimensional; 3DGeo_CT, 3-dimensional geometry derived from computed tomographic imaging; OCT = optical coherence tomography.

determine the optimal tool combinations for accurate navigation and to troubleshoot real-time colocalization techniques (animals #1 and #2). The second phase entailed the delivery of vascular stents to computer-generated (virtual) targets intended to mimic arterial lesions (animals #3 to #6). The third phase entailed the delivery of long stents over shorter stents, the latter being used as nonvirtual, quantifiable targets (animal #6).

Healthy Yorkshire swine (median weight 36 kg; range: 33-40 kg) were studied. In each animal, stent delivery was attempted in either the left or right carotid artery and in the left anterior descending coronary artery. Both carotid and coronary territories were studied in the same animals to satisfy the premise for the smallest number of animals required

to obtain valid information in accordance with the "3 R's" tenet—replacement, reduction, and Refinement—to maximize the welfare of the animals (12). Animals were induced with tiletamine/zolazepam (12 mg/kg intramuscular), intubated, anesthetized with isoflurane (3.5%), and ventilated, as previously reported (13). Anticoagulation was maintained with unfractionated heparin. Blood pressure, electrocardiogram, and oxygen saturation were continuously monitored during the entire procedure. Animals were euthanized immediately after the last stent implantation. Experiments were performed in accordance with the Canadian Council on Animal Care guidelines for animal experimentation and were approved by the Montreal Heart Institute's Animal Care and Use Committee.

COMPUTED TOMOGRAPHIC IMAGING AND SEGMENTATION. Computed tomographic angiography (CTA) was performed prior to the intervention using a dual-energy scanner (256 slices; Siemens Definition Flash, Siemens Healthcare), using a rotation time of 280 ms at a temporal resolution of 75 ms and 0.6-mm collimation. For carotid arteries, Isovue 370 (Bracco Diagnostics; 80 mL at 5.0 mL/s) was injected through a central venous line. Images were acquired from the proximal ascending aorta to the base of the skull (dual-energy mode; 90 kVp and Sn 150 kVp). For the coronary arteries, animals were pretreated with intravenous metoprolol (5 mg every 5 minutes, for a total of 25 mg) and inhalational nitroglycerin (0.8 mg, 2 minutes before acquisition) and thereafter injected with Isovue 370 (77 mL at 5.5 mL/s). Acquisition was performed with high-pitch prospective electrocardiographic gating (FLASH) (tube voltage 70 kV). Important vascular structures (left ventricle, coronary arteries, aorta, and carotid arteries) were segmented and reconstructed in 3 dimensions from computed tomographic slices using EnSite Verismo software (Abbott Medical).

NAVIGATION SYSTEM AND CARDIAC REGISTRATION. The EnSite Velocity cardiac mapping system (Abbott Medical) is a catheter navigation and mapping system capable of displaying the 3D position of conventional catheters, as well as displaying cardiac electric activity as waveform traces and as dynamic 3D isopotential maps.

Prior to tool navigation, 3D geometry derived from computed tomographic imaging ($3DGeo_{CT}$) was integrated in an impedance-based navigation system (EnSite Velocity) (**Figures 1B and 2A**) through a fiducial-based registration process. A 6-F decapolar diagnostic catheter (Livewire, Abbott) was initially positioned in the right atrium and served as a steady central reference point for precise tool localization. A second decapolar catheter was used with fluoroscopy to create a primary 3D geometry in the navigation system and locate specific anatomic landmarks to be used for registration (right and left aortic cups near coronary ostia, origin of the brachiocephalic trunk, and origin of the left and right common carotid arteries). Between 25 and 30 fiducial points were generated to link the coordinate systems of the navigation system and the $3DGeo_{CT}$ and to ensure an accurate registration process (Fusion feature, Abbott) to enable the navigation of modified tools in the $3DGeo_{CT}$. A smaller guidewire was used for $3DGeo_{CT}$ registration of the coronary arteries.

GUIDEWIRE AND CATHETER NAVIGATION. Electrically insulated guidewires were modified to become accurately detectable in the navigation system and to inform the operator of the distal position of the intervention wire (**Figure 2A**). Rapid-exchange monorail stent catheters were also adapted to fit distal electrodes connectable to the navigation system. To this end, customized insulated 0.014-inch electrodes with bare distal tips were crimped between the balloon catheter and the distal stent margin (**Figure 2B**). These electrodes allowed real-time and precise localization of tools within the navigated arteries. Each modified tool was individually calibrated using standard angiography and fluoroscopy to confirm proper anatomical-impedance coupling before delivery. The accuracy and precision of the customized electrodes for navigation within the EnSite mapping system were measured against a fluoroscopic standard.

PERCUTANEOUS CORONARY AND CAROTID INTERVENTIONS WITH NO CONTRAST MEDIUM OR X-RAYS. As healthy animals do not display atherosclerosis, arterial lesions had to be generated by computer on the $3DGeo_{CT}$ and used as targets for stent delivery (phase 2). These virtual targets were prespecified in length and distance from a distinct vascular landmark (bifurcation, large branch) visible both on the $3DGeo_{CT}$ and conventional angiography. Vascular landmarks were used as reference to confirm proper stent positioning with angiography at procedure end. For carotid intervention, the bifurcation carina between the left and the right common carotid arteries was systematically used as the landmark. For coronary intervention, the left main bifurcation and diagonal bifurcation (first or second) were used as landmark for percutaneous coronary intervention in the circumflex and left descending coronary arteries, respectively.

Distances in millimeters were measured on $3DGeo_{CT}$ from the anatomical landmark to define the target lesion (**Figures 3A and 4A**). For stent sizing, data derived from the computed tomographic scan were used. Intervention wires and stents were then navigated toward the virtual target for alignment and implanted with no fluoroscopy or contrast medium. After stenting of the left anterior descending coronary artery, optical coherence tomographic (OCT) imaging was performed using a dedicated catheter (Dragonfly Optis, Abbott Vascular) using a heparinized saline flush instead of radiographic contrast, as previously reported (14). OCT imaging was not attempted in the carotid arteries, because of the vessel's large diameter. Once the intervention was deemed completed with the navigation system, patency of the target arteries and stent position were

FIGURE 2 Detection Methods for Stent Navigation

A The navigation system
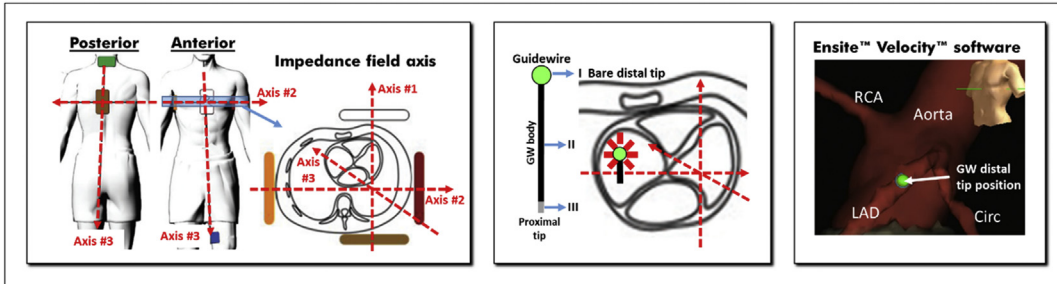
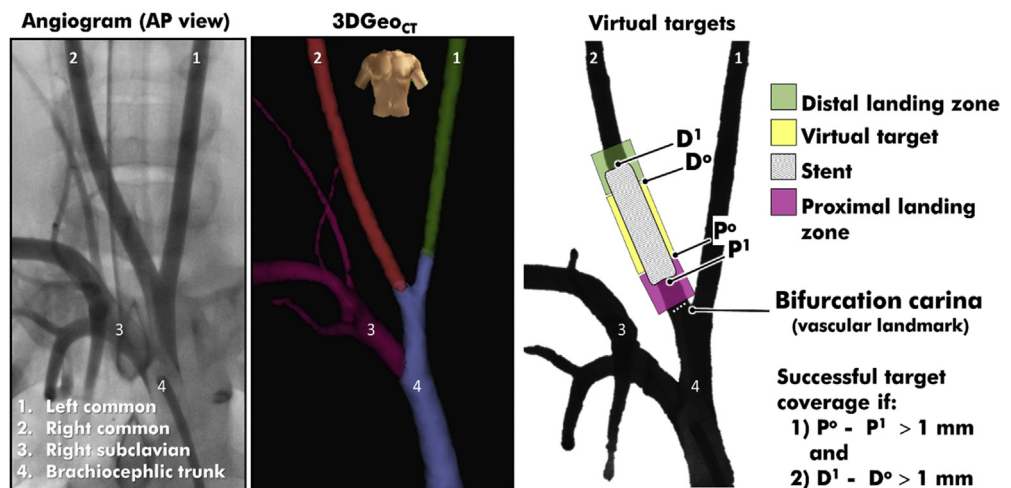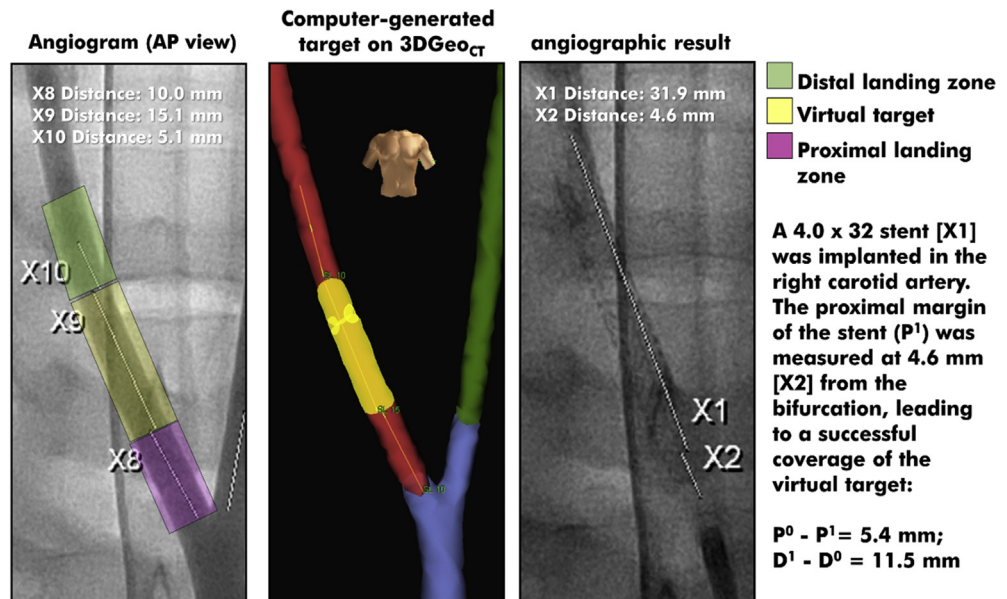**B** Tool modification for detection in the navigation system
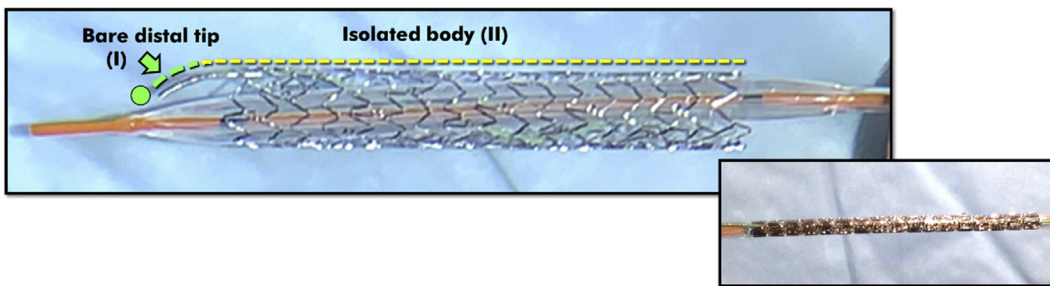
(A) Impedance navigation principle of the EnSite Velocity mapping system uses 3 pairs of patches to define the navigation coordinate axes (axis #1, anteroposterior; axis #2, right-left; axis #3, craniocaudal) **(left)**. Tools can be detected with a metallic probe made of a bare tip (uncoated metal) at the distal end (I on the electrode) followed by a coated (and thus electrically isolated) shaft (II on the guidewire [GW]) and ending with an uncoated/exposed tip at the proximal end outside the animal (III on the guidewire) **(middle)** to enable connection to the navigation system **(right)**. **(B)** Insertion and crimping of a modified 0.014-inch electrode underneath a stent makes detection in the navigation system possible. The electrode **(green arrow)** is located at a specified distance from the distal margin of the stent. The distal bare tip is short (2 mm) and becomes the detection point **(green dot in A, middle and right)** in the navigation system. The shaft of the electrode **(yellow dotted line)** is electrically insulated and therefore is not detected in the navigation system. Circ = circumflex coronary artery; LAD = left anterior descending coronary artery; RCA = right coronary artery.

confirmed on conventional angiography. Stent sizes and distances between stents and vascular landmarks were measured using quantitative coronary angiography (Syngo VC21C, Siemens). Measurements were made in triplicate and averaged.

In the last animal (phase 3 experiments), short stents were deployed on virtual targets in the left carotid artery and the left anterior descending coronary artery (as described previously), and stent-in-stent deployments were then attempted. In such cases, longer stents were implanted over the shorter stents, which were used as tangible and quantifiable targets. The short stents were located in 3DGeo$_{CT}$, and the longer stents were then navigated to cover both the proximal and the distal margins of the shorter, deployed stent.

PROCEDURAL SUCCESS AND ENDPOINTS. In phase 2 (computer-generated targets), procedural success was defined as complete coverage of virtual targets by

the stents with appropriate sizing and vessel wall apposition, free of edge dissection. Target coverage was ascertained using quantitative coronary angiography using the distances between the distal stent margin and the vascular landmark (**Figures 3A and 4A**, top). Quantitative coronary angiographic distances were compared with the distances derived from the navigation system (computed from positional markers' Cartesian coordinates). Euclidian distance computation provided the final measurement values. In coronary arteries, stent apposition to the vessel wall was quantified on OCT imaging by measuring the distance between the abluminal stent side and the vessel wall. The area of malapposition was calculated for each OCT cross-sectional slice by subtracting the stent surface area from the vessel lumen area in nonbifurcated segments. Edge dissections were defined using established criteria (15). In phase 3 (stent-in-stent targets), procedural success was

FIGURE 3 Definition of Virtual Target and Successful Stent Implantation With No Contrast Medium or X-Ray Use in the Right Carotid Artery

A Definition of the virtual target in the right carotid artery

Angiogram (AP view)
3DGeo$_{CT}$
Virtual targets

1. Left common
2. Right common
3. Right subclavian
4. Brachiocephlic trunk

Distal landing zone
Virtual target
Stent
Proximal landing zone

Bifurcation carina (vascular landmark)

Successful target coverage if:
1) $P^0 - P^1 > 1$ mm and
2) $D^1 - D^0 > 1$ mm

B Successful Stent Implantation with no contrast medium or x-ray

Angiogram (AP view)
Computer-generated target on 3DGeo$_{CT}$
angiographic result

X8 Distance: 10.0 mm
X9 Distance: 15.1 mm
X10 Distance: 5.1 mm

X1 Distance: 31.9 mm
X2 Distance: 4.6 mm

Distal landing zone
Virtual target
Proximal landing zone

A 4.0 x 32 stent [X1] was implanted in the right carotid artery. The proximal margin of the stent (P^1) was measured at 4.6 mm [X2] from the bifurcation, leading to a successful coverage of the virtual target:
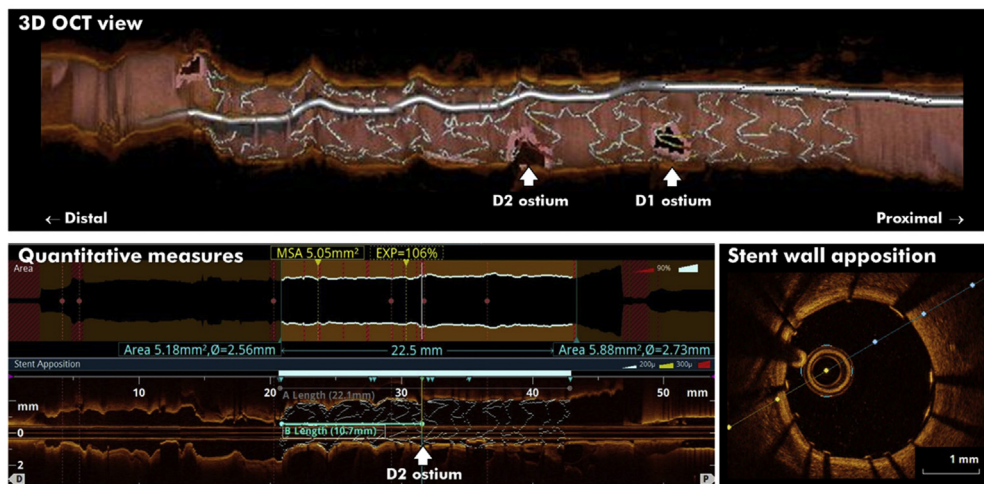
$P^0 - P^1 = 5.4$ mm;
$D^1 - D^0 = 11.5$ mm

(A) The right carotid virtual target defined in 3-dimensional geometry derived from computed tomographic imaging (3DGeo$_{CT}$) near the bifurcation where the carina is used as the vascular landmark. Distances between the carina and the proximal (P^0) and distal (D^0) margins of the target (in **yellow**) were compared with the distances between the carina and the proximal (P^1) and distal (D^1) margins of the stent. Target coverage was deemed successful if 1) $P^0 - P^1 > 1$ mm; and 2) $D^1 - D^0 > 1$ mm. **(B)** The virtual target was defined on the reference angiogram as starting 10 mm distal from the common carotid carina (P^0 = 10mm, seen as X8 on quantitative coronary angiography [QCA]) and was set to measure 15 mm (seen as X9 on QCA), leading to D^0 = 25 mm **(left)**. The target was generated by computer on the 3DGeo$_{CT}$ **(middle)**. A 4.0 × 32 mm stent (seen as X1 on QCA) was implanted with no contrast medium or fluoroscopy. The proximal margin of the stent was measure at 4.6 mm from the bifurcation (seen as X2 on QCA), leading to successful coverage ($P^0 - P1 = 5.4$ mm, $D^1 - D^0 = 11.5$ mm) **(right)**. AP = anteroposterior view.

FIGURE 4 Definition of Virtual Target and Successful Stent Implantation With No Contrast Medium or X-Ray Use in the LAD
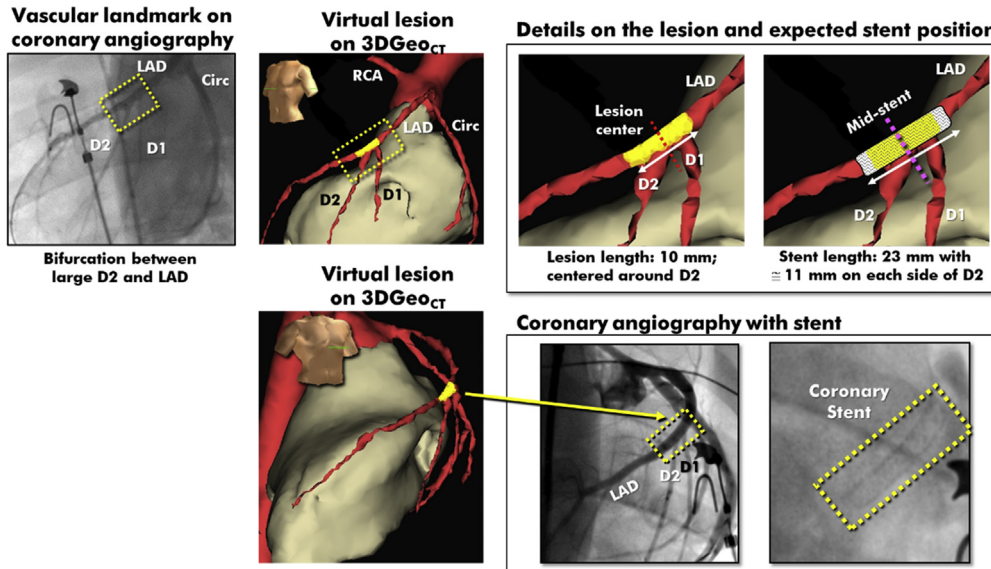
(A) The virtual target was centralized in 3DGeo$_{CT}$ at the origin of the second diagonal branch (D2) and was set to measure 10 mm (P^O = −5 mm, D^O = +5 mm). A 3.0 × 23 mm stent delivered with successful coverage (P^1 = −11.5 mm, D^1 = +11.5 mm). The final coronary angiogram shows an expanded stent centrally positioned over the second diagonal. (B) The longitudinal and cross-sectional optical coherence tomographic views show complete (93.8% ± 1.8%) wall apposition throughout the stent. The quantitative measurements confirm proper position of the distal margin of the stent, measured at 10.7 mm (or 48% of the total stent length) from the center of the virtual target. D = diagonal; OCT = optical coherence tomographic; PCI = percutaneous coronary intervention; other abbreviations as in **Figures 1 and 2**.

defined as the both the proximal and distal margins of the second longer stent covering the proximal and distal margins of the shorter stent. Other procedural endpoints included: 1) the accuracy of the navigation system; 2) the time for 3D geometry integration and fusion (in minutes); and 3) the time for stent implantation with the navigation system (in seconds).

ACCURACY OF CUSTOMIZED ELECTRODES. To determine whether customized electrodes could accurately track devices in the navigation system, we

FIGURE 5 **Metrics of Procedural Success**

A **Procedural learning curve**

B **Bland Altman plot with limits of agreement of the differences between QCA vs. EnSite distances**

(A) The steep learning curve suggests that interventionalists familiarized with the navigation system can aim precisely at identified targets. **(B)** Distances between the vascular landmark and the distal margin of the stent were measured using quantitative coronary angiography (QCA) and strongly agreed with the Euclidean distances derived with the navigation system (intraclass correlation coefficient = 0.96; 95% confidence interval: 0.86 to 0.99; $P < 0.01$).

compared the distances derived in the EnSite mapping system with those measured on fluoroscopy (the gold standard). To this end, we used 2 radiopaque markers known to be 10 mm apart on a decapolar catheter (Livewire) as a fluoroscopic reference. The decapolar catheter was positioned in the left carotid artery, and the customized electrode was retracted under fluoroscopic guidance from the distal to the proximal radiopaque markers over 10 mm. This measurement was repeated 10 times. Before and after each pull back, the electrode's x, y, and z coordinates were derived in EnSite and used to measure Euclidean distances. Euclidean distances were chosen to eliminate human error in repeated measurements. Additionally, to minimize the variations caused by thoracic movements during breathing, 5 measurements were performed during forced apnea (by disconnecting the respirator for 10 seconds, under deep sedation) and 5 measurements were performed during the thoracic death (end-expiratory) time.

DATA PROCESSING AND STATISTICAL ANALYSIS. Continuous variables are expressed as mean ± SD, median (interquartile range [IQR]), or range. Categorical variables are presented as number (percentage). Intraclass correlation coefficients were used to assess the relationship between continuous variables. As this was a proof-of-concept study, the sample size was not hypothesis driven, and therefore no

assumption is presented. Rather, the sample size was determined by the team's experience in large animals and confidence to achieve successful implantation on the basis of early experiments on a dedicated imaging phantom. Statistical analyses were performed using SPSS version 24 (IBM). Accuracy is expressed with the coefficient of variation (calculated as the SD divided by the mean Euclidean distance, expressed as a percentage) and defined as (100% − coefficient of variation). Precision was defined as the 95% confidence interval around the mean Euclidean distance.

RESULTS

SUCCESS OF PROCEDURAL GUIDANCE. In phase 1, customized tools (electrodes, stents, OCT catheters) were optimized, calibrated, and used for navigation in the carotid and coronary vasculature. As part of this phase, no stent implantation or OCT imaging could be successfully accomplished without using contrast medium or x-rays. The insertion of the customized probe led variously to inadequate stent crimping, vessel encroachment, dissection, and thrombosis. These problems were solved by returning to the bench to develop a properly isolated probe with a shorter, softer distal bare tip. This yielded a profiled, atraumatic delivery system with superior navigation properties suitable for blind navigation. Phase 2 then saw a notable evolution in the devices and

FIGURE 6 Successful Stent-in-Stent Implantations in the Left Carotid Artery
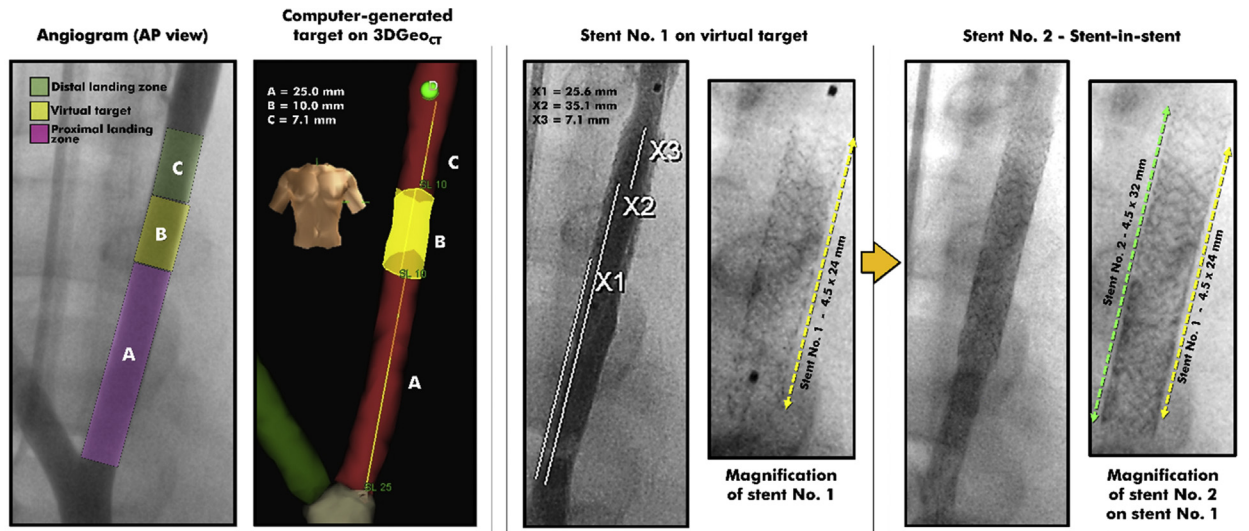
Using the carotid bifurcation as a vascular landmark, a target **(yellow, in left panel)** was generated in 3DGeo$_{CT}$. Stent #1 (4.5 × 24 mm) was successfully delivered over the virtual target. Quantitative coronary angiographic measures X1 and X2 mark the proximal and distal margins of the virtual target, at 25 and 35 mm from the bifurcation (for a total length of 10 mm). X3 marks the distal margin of the stent #1, which is at 7.1 mm above the distal margin of the virtual lesion. The position of stent #1 was updated in 3DGeo$_{CT}$, and stent #2 (4.5 × 32 mm) could be delivered within stent #1, with no contrast medium or x-rays. The final angiogram shows stent #2 centered on stent # 1 **(right)**. Abbreviations as in **Figures 1 and 3**.

implantation techniques, which translated into a steep acceleration of procedural successes (**Figure 5A**). Stents were successfully implanted in 9 of the 11 attempted targets (82%) (7 carotid and 4 coronary arteries). Examples of successful interventions in the carotid and coronary arteries are shown in **Figures 3B and 4A** (bottom) and **4B**, respectively. When used in the coronary arteries, saline-flush OCT imaging confirmed appropriate sizing and complete stent apposition (**Figure 4B**). In the last 2 animals, 6 of the 7 attempted interventions were successful, including 2 stent-in-stent implantations (**Figure 6**). Procedural failures occurred in the carotid arteries of 2 distinct animals and resulted from misalignments of the stent with the virtual lesion. This is assumed to be the result of an inadequate calibration of the probe before the stent implantation.

PROCEDURAL PRECISION AND TIME REQUIRED. Compared with a 10-mm fluoroscopic standard, the mean Euclidean distance measured with the EnSite mapping system was 9.92 ± 0.90 mm (range: 8.56-11.99 mm). The accuracy was measured at 90.9%. Precision was estimated at ±1.4 mm, which means that we were 95% confident that a point located in the electroanatomical navigation system EnSite was within 1.4 mm of the location that would have been provided by fluoroscopy.

Following stenting, the Euclidean distances measured from data exported from the EnSite mapping system between the vascular landmark and the distal margin of the stent (where the customized electrode was inserted) agreed strongly with the same distances measured on quantitative coronary angiography (intraclass correlation coefficient = 0.96; 95% confidence interval: 0.86-0.99; $P <$ 0.01) (**Figure 5B**). Of the 11 distances available, the difference between EnSite and quantitative coronary angiography was <2 mm in 3 instances, between 2 and 6 mm in 5 instances, and >6 mm in 3 instances (2 of which were procedural failures).

The integration of 3D geometries derived from imaging modalities added a median of 23 minutes (IQR: 21-25 minutes) to carotid interventions and 8 minutes (IQR: 7-10 minutes) to coronary interventions. The time allocated to geometry integration declined steadily as the team gained experience. The median navigation time required for stenting was 8 second (IQR: 6-12 seconds) in the carotid arteries and 17 seconds (IQR: 13-21 seconds) in the coronary arteries.

DISCUSSION

In this proof-of-concept study, we have demonstrated that a navigation system can be used to

integrate information from multiple modalities, including preprocedural cross-sectional imaging, to navigate diagnostic and interventional tools safely within carotid and coronary arteries and to deliver therapeutic devices precisely to targeted arterial segments. Our experiments led to the implantation of stents in coronary and carotid arteries with appropriate sizing and wall apposition without using additional contrast and x-rays beyond what was necessary for the CTA and anatomical mapping. This innovative approach has important clinical implications, given the growing role played by noninvasive imaging modalities in the primary stratification of patients with stable ischemic heart disease and symptomatic cerebrovascular disease and the increasing emphasis on avoidance of the hazards related to x-ray and contrast medium use.

As suggested by our steep learning curve, we can reasonably expect that properly trained interventional cardiologists will rapidly become comfortable with using navigation systems during intervention, as were electrophysiologists in the past (16). Nair et al (10) recently showed the feasibility of navigation of an angioplasty catheter to lesion site using the EnSite navigation system. Similarly, the efficiency of our image integration method increased with each additional animal completed but remains to be improved; as a comparison, Brooks et al (17) reported a significant decrease of the fusion time in electrophysiology cases after only 15 patients. Upon availability of novel tools, dedicated devices, and capitalizing on past experiences in cardiovascular navigation (18-20), the operator's experience can only improve. In addition to tool guidance, the navigation systems allow the integration of preprocedural data from noninvasive imaging modalities, which can be linked with periprocedural data acquired by the system. This may lead navigation systems toward a more central role in percutaneous vascular interventions. The rapid evolution of imaging technology (molecular imaging, coronary flow simulation, etc) has led CTA to play an expanding role in the risk stratification (21) of patients with stable ischemic heart disease. Progression of computed tomographic angiographic data resolution does provide high-quality preprocedural data to physicians and may become a modality of choice to diagnose obstructive coronary artery disease (22). In parallel, cardiovascular magnetic resonance (CMR) is rapidly evolving (23). The navigation system used in this experiment has the capacity to merge any CTA or CMR angiography into live 3D geometries for interventions with minimal use of fluoroscopy. In electrophysiology ablation procedures, preprocedural image integration has been associated with a reduction in fluoroscopy time (17) and an improvement in positive clinical outcomes (24).

In addition to preprocedural data merging, modern navigation systems have the capacity to track and coregister OCT or intravascular ultrasound catheters to enable low-contrast image-guided interventions (4). Bridging preprocedural (noninvasive cross-sectional imaging; eg, computed tomography, CMR) with periprocedural (viability maps, fractional flow reserve, resting full cycle ratio, coronary flow reserve) data through integration in a navigation system has the potential to be the missing integrative concept for maximal leveraging of all data generated for a given patient. Such an integrative concept leads us to foresee vascular stenting procedures free of the obligation to use either iodine-based contrast or x-rays in the near future while simultaneously clinically assessing the vascular network and associated myocardial substrate. An improved understanding of the link between these 2 aspects could manifestly also help assess the impact of revascularization in ventricular arrhythmias (25), thereby feeding back the benefits of such navigations into the therapy area for which they were originally designed. Additional research and technological refinements will be required before such navigation systems can be used in routine clinical practice.

STUDY LIMITATIONS. In 2 attempted interventions, we experienced a significant drift in the position (coordinates), which was likely caused by an unstable impedance signal. Impedance-based navigation systems were designed for electrophysiology mapping in wide cardiac chambers (as opposed to tubular arteries), and an open mapping system architecture was more amenable to visualize jury-rigged tools and thus provided the needed flexibility in our tool optimization process to show proof of concept. Periprocedural impedance variations, notably caused by important saline injection, did affect EnSite's tracking ability in our experiments and required correction by adding fiducial merging points. Fusion of $3DGeo_{CT}$ and fiducial points were the main drivers for the system impedance-based accuracy in this study. Future refinements of the methodology should include more stable and precise magnetic-based localization mapping systems. The vascular geometry building process required a greater number of tool passes to achieve a reasonable outcome. Given the vascular network configuration (linear, smaller volumes) and associated pathologies (obstructed vessel lumen), multiple vascular passes for geometry improvement will not be a viable clinical option. Challenges related to geometry creation did limit the application of the field-scaling algorithm identified as an important

component in cardiac chamber fusion process. Appropriate field scaling application on vascular geometries could help increase navigation accuracy and reduce the number of fiducial points required in the fusion process. In tortuous or calcified arteries, the techniques described in this report will likely help minimize the amount of contrast and x-rays required to perform an intervention but are unlikely to replace standard tools and imaging systems.

CONCLUSIONS

On the basis of this preclinical proof-of-concept study, we suggest that navigation systems can be used to assist interventionalists to perform coronary stenting or carotid intervention while minimizing x-ray and contrast use and thereby reducing risk to patients and health care professionals alike. Such a disruptive approach has the potential to leverage noninvasive imaging, already being used in patient stratification, to alter fundamentally the way vascular interventions are performed in the future.

FUNDING SUPPORT AND AUTHOR DISCLOSURES

ADDRESS FOR CORRESPONDENCE: Dr E. Marc Jolicoeur, Centre Hospitalier de l'Université de Montréal, Service de Cardiologie Interventionnelle, 1051 rue Sanguinet, Montréal, Québec H2X 3E4, Canada. E-mail: marc.jolicoeur@umontreal.ca.

PERSPECTIVES

COMPETENCY IN MEDICAL KNOWLEDGE Interventional cardiologists and radiologists rely on fluoroscopy and contrast media to perform percutaneous interventions. Emerging technologies exist that may one day reduce the need for harmful x-rays or contrast. This would render stenting safer for both patients and medical teams performing interventions.

TRANSLATIONAL OUTLOOK: An important proportion of patients with coronary artery disease are screened noninvasively with CMR imaging or coronary CTA. Navigators can integrate anatomical data with topographic maps of ischemia, viability, and contractility gathered from other imaging modalities to create a multilayered map for intervention. In the future, when angioplasty is deemed necessary, customized imaging catheters and angioplasty devices could be tracked inside patients using electromagnetic detection superposed to the multilayered maps outlined in the navigator. These maps, combined with electromagnetic navigation, could be used to reduce x-ray and contrast medium use during traditional or robotic-assisted percutaneous intervention and guide proper decisions during revascularization.

REFERENCES

1. Eisenberg MJ, Afilalo J, Lawler PR, Abrahamowicz M, Richard H, Pilote L. Cancer risk related to low-dose ionizing radiation from cardiac imaging in patients after acute myocardial infarction. *CMAJ*. 2011;183:430–436.

2. Attigah N, Oikonomou K, Hinz U, et al. Radiation exposure to eye lens and operator hands during endovascular procedures in hybrid operating rooms. *J Vasc Surg*. 2016;63:198–203.

3. Reeves RR, Ang L, Bahadorani J, et al. Invasive cardiologists are exposed to greater left sided cranial radiation: the BRAIN study (Brain Radiation Exposure and Attenuation During Invasive Cardiology Procedures). *J Am Coll Cardiol Intv*. 2015;8: 1197–1206.

4. Ali ZA, Karimi Galougahi K, Nazif T, et al. Imaging- and physiology-guided percutaneous coronary intervention without contrast administration in advanced renal failure: a feasibility, safety, and outcome study. *Eur Heart J*. 2016;37:3090–3095.

5. Li Z, Zhou Y, Xu Q, Chen X. Staged versus one-time complete revascularization with percutaneous coronary intervention in STEMI patients with multivessel disease: a systematic review and meta-analysis. *PLoS ONE*. 2017;12:e0169406.

6. Mahmud E, Schmid F, Kalmar P, et al. Feasibility and safety of robotic peripheral vascular interventions: results of the RAPID trial. *J Am Coll Cardiol Intv*. 2016;9:2058–2064.

7. Sommer P, Bertagnolli L, Kircher S, et al. Safety profile of near-zero fluoroscopy atrial fibrillation ablation with non-fluoroscopic catheter visualization: experience from 1000 consecutive procedures. *Europace*. 2018;20:1952–1958.

8. Aryana A, Cavaco D, O'Neill PG, Dinh HH, Bowers M, D'Avila A. Three-dimensional electroanatomical mapping to guide endocardial occlusion of stenotic left atrial appendage. *J Innov Cardiac Rhythm Manage*. 2014;5:8.

9. Razminia M, Willoughby MC, Demo H, et al. Fluoroless catheter ablation of cardiac arrhythmias: a 5-year experience. *Pacing Clin Electrophysiol*. 2017;40:425–433.

10. Nair M, Singal G, Yaduvanshi A, Kataria V. First in man: percutaneous coronary angioplasty using non-fluoroscopic electro-anatomic mapping. *Int J Cardiovasc Imaging*. 2020;36:1189–1190.

11. Weisz G, Smilowitz NR, Moses JW, et al. Magnetic positioning system in coronary angiography and percutaneous intervention: a feasibility and

safety study. *Catheter Cardiovasc Interv*. 2013;82: 1084–1090.

12. Fenwick N, Griffin G, Gauthier C. The welfare of animals used in science: how the "three Rs" ethic guides improvements. *Can Vet J*. 2009;50:523–530.

13. Banai S, Jolicoeur EM, Schwartz M, et al. Tiara: a novel catheter-based mitral valve bioprosthesis: initial experiments and short-term pre-clinical results. *J Am Coll Cardiol*. 2012;60:1430–1431.

14. Kendrick DE, Allemang MT, Gosling AF, et al. Dextran or saline can replace contrast for intravascular optical coherence tomography in lower extremity arteries. *J Endovasc Ther*. 2016;23:723–730.

15. Räber L, Mintz GS, Koskinas KC, et al. Clinical use of intracoronary imaging. Part 1: guidance and optimization of coronary interventions. An expert consensus document of the European Association of Percutaneous Cardiovascular Interventions. *Eur Heart J*. 2018;39:3281–3300.

16. Chen G, Wang Y, Proietti R, et al. Zero-fluoroscopy approach for ablation of supraventricular tachycardia using the Ensite NavX system: a

multicenter experience. *BMC Cardiovasc Disord.* 2020;20:48.

17. Brooks AG, Wilson L, Kuklik P, et al. Image integration using NavX Fusion: initial experience and validation. *Heart Rhythm*. 2008;5:526–535.

18. Lima da Silva G, Cortez Dias N, Carpinteiro L, de Sousa J. Electroanatomical mapping of coronary artery anatomy to guide epicardial ventricular tachycardia ablation. *Europace*. 2018;20:419.

19. Piorkowski C, Arya A, Markovitz CD, et al. Characterizing left ventricular mechanical and electrical activation in patients with normal and impaired systolic function using a non-fluoroscopic cardiovascular navigation system. *J Interv Cardiac Electrophysiol*. 2018;51:205–214.

20. Kawata H, Yamada T, Karanam S, Reddy R. Intracoronary artery mapping and 3-dimensional visualization of the coronary arteries with a 0.014 inch guidewire in catheter ablation of left ventricular summit premature ventricular contractions. *HeartRhythm Case Rep*. 2020;6:914–917.

21. Newby DE, Adamson PD, Berry C, for the SCOT-HEART Investigators. Coronary CT angiography and 5-year risk of myocardial infarction. *N Engl J Med*. 2018;379:924–933.

22. Knuuti J, Wijns W, Saraste A, et al. 2019 ESC guidelines for the diagnosis and management of chronic coronary syndromes: the Task Force for the Diagnosis and Management of Chronic Coronary Syndromes of the European Society of Cardiology (ESC). *Eur Heart J*. 2019;41:407–477.

23. Arnold JR, McCann GP. Cardiovascular magnetic resonance: applications and practical considerations for the general cardiologist. *Heart*. 2020;106:174–181.

24. Yamashita S, Cochet H, Sacher F, et al. Impact of new technologies and approaches for post-myocardial infarction ventricular tachycardia ablation during long-term follow-up. *Circ Arrhythm Electrophysiol*. 2016;9:e003901.

25. Mondesert B, Khairy P, Schram G, et al. Impact of revascularization in patients with sustained ventricular arrhythmias, prior myocardial infarction, and preserved left ventricular ejection fraction. *Heart Rhythm*. 2016;13:1221–1227.